Ab initio study of *h*-BN nanomeshes on Ru(001), Rh(111), and Pt(111)

Robert Laskowski and Peter Blaha
Institute of Materials Chemistry, Technische Universität Wien, Getreidemarkt 9/165TC, A-1060 Vienna, Austria
(Received 14 December 2009; revised manuscript received 25 January 2010; published 17 February 2010)

The atomic and electronic structure of *h*-BN deposited on Ru(001), Rh(111), and Pt(111) is discussed in terms of *ab initio* density functional theory. Our calculations indicate that the interaction between *h*-BN and the metal substrate is relatively weak for the *h*-BN/Pt(111) interface but rather strong for the Ru(001) and Rh(111) surfaces. The corrugations of the *h*-BN layer calculated for *h*-BN/Rh(111) and *h*-BN/Ru(001) are comparable and much larger than the one found for *h*-BN/Pt(111) interface. We show that the core, as well as the valence states of *h*-BN, is rigidly shifted in energy and this shift depends on the distance of the *h*-BN from the metal atoms. The states localized on atoms in "high" (nonbounding) nanomesh regions are shifted upward in energy relative to the "low" (bounding) regions. Moreover the actual magnitudes of the shifts are quite similar for all three interfaces. We can correlate this shift with the nonuniform charge transfer from the *h*-BN layer which results in the development of the nonuniform electrostatic field above the overlayer.

DOI: 10.1103/PhysRevB.81.075418 PACS number(s): 73.20.At, 73.22.−f

I. INTRODUCTION

Hexagonal boron nitride (*h*-BN) is well known to bond to many transition metal (TM) surfaces forming well-ordered and uniform monolayers. For commensurate interfaces, when the lattice sizes of the overlayer and the metal surface match [such as Ni(111) (Ref. 1) and Cu(111) (Ref. 2)] the N atom stays on top of the metal atom and the B atom can occupy both the hcp or fcc positions. The (B-fcc, N top) configuration results in a slightly lower total energy.[3] Even when the interaction between *h*-BN and the substrate is considered to be relatively strong,[2,4] it does not weaken considerably the rigid sp^2 bonds between N and B in the hexagonal plane.[5] Therefore, when *h*-BN is deposited on lattice-mismatched interfaces such as Rh(111),[6] Ru(001),[7,8] Pt(111),[8–10] and Pd,[11] the N-B bond length is close to the one in free *h*-BN, and a highly regular mesh with a periodicity of a few nanometers develops, which is compatible with both the BN and the TM substrate lattice constants. The lattice size of the substrate is usually larger than the *h*-BN lattice constant by a few percent. To some extend these nanostructures can be viewed as a kind of Moiré pattern that arise due to the lattice mismatch and the resulting modulation of the interaction between the *h*-BN monolayer and the substrate. However, in the Rh(111) and Ru(001) cases the electronic properties of these nanostructures are very strongly affected by the formation of the pattern.[7,12] Moreover, the *h*-BN is not flat but has a rather large corrugation (1–2 Å). Therefore, in order to emphasize that such nanostructures are often much more than just weak visual effects in scanning tunneling microscopy (STM) images, they are referred in literature as "nanomesh." Such interfaces become a very interesting class of materials that can serve as nanoscale templates for trapping of molecules or clusters. For instance, it has been shown that *h*-BN films deposited on Ru(0001) (Refs. 7 and 13) or Rh(111) (Ref. 14) can accommodate Au clusters, but also regular arrays of Co clusters[15] or naphthalocyanine molecules have been successfully deposited on the *h*-BN/Rh(111) nanomesh.[6] Formation of similar patterns has also been observed for other overlayers than *h*-BN. They appear, for example, when graphene is deposited on transition metal surfaces,[16–19] as well as for the FeO/Pt(111) (Ref. 20) interface. It has also been reported that *h*-BN can be deposited on surfaces with other than hexagonal symmetry. For example, in a case of Cr(110) (Ref. 21) and Mo(110) (Ref. 22) one-dimensional nanostructures appear. Due to coincidence in lattice size of *h*-BN and the Pd(111) and Pt(111) surfaces a distinct structure denoted by $\sqrt{3}\times\sqrt{3}$-*R*30° can also appear[10,11] where the BN unit is rotated by 30° with respect to the substrate.

Due to the strong coupling between the Moiré pattern and the electronic structure in the *h*-BN/Rh(111) interface, a very different atomic structure has been proposed previously. In order to explain the observed σ band splitting and STM images, initially Corso *et al.*[12] suggested that the *h*-BN/Rh(111) nanomesh consists of two incomplete *h*-BN layers. However, it has been shown later that a single monolayer model of *h*-BN on Rh(111) with a highly corrugated *h*-BN layer can also explain the experimentally observed σ band splitting and STM images.[23,24] The unit cell in this case consists of a 13×13 supercell of *h*-BN monolayer and a 12×12 supercell of the Rh(111) surface. Moreover the monolayer is not flat but is highly corrugated, i.e., undergoes strong vertical deformation. Further experiments supported the single layer model of *h*-BN/Rh(111).[6] The actual size of the supercell may depend on the growth conditions; for example, Müller *et al.*[25] reported evidence for a structure with periodicities of 14×14 *h*-BN and 13×13 Rh cells, but qualitatively the structure is unchanged. The theoretical and experimental investigations lead to a more unified picture of the whole class of *h*-BN/TM interfaces, such that there are no qualitative differences between different substrates. This issue was addressed by, e.g., Preobrajenski *et al.*[26] They showed with core level spectroscopies [near-edge x-ray-absorption fine structure and photoelectron spectroscopy (PES)] that the properties of *h*-BN change gradually when it is adsorbed on Ru(0001), Rh(111), Ir(111), and Pt(111). They found that Ru(111) and Rh(111) are affecting the *h*-BN layer much stronger than Ir(111) and Pt(111) and therefore concluded that *h*-BN bonding to the substrate is much stronger for

Ru(111) and Rh(111) than for Ir(111) and Pt(111).

In this work we discuss the properties of *h*-BN adsorbed on Ru(001), Rh(111), and Pt(111) surfaces in terms of *ab initio* density functional theory (DFT) calculations. We focus on the differences in atomic and electronic structure between the interfaces and compare our results with the experiments of Preobrajenski *et al.*[26] We also give an explanation for the observed shifts of the electronic levels between different regions of the nanomeshes. The *h*-BN layer is nonuniformly charged, and this results in a nonuniform electrostatic field above the layer, explaining the observed level shifts.

II. RESULTS AND DISCUSSION

A. Atomic structure of the *h*-BN overlayer

The DFT *ab initio* calculations presented in this work have been performed with the WIEN2K code[27] which implements the augmented plane wave plus local orbital method[28] in the DFT. We have used the Wu-Cohen (WC) generalized gradient approximation (GGA) version of GGA,[29] which is a good compromise between local-density approximation (LDA) and Perdew, Burke, Ernzerhof (PBE) version of GGA.[30,31] The Rh(111) and Pt(111) interfaces are composed of three metal layers covered from both sides by a monolayer of *h*-BN. For *h*-BN/Ru(001) four layers of metal are used because of the hcp stacking. This setup allows us to utilize inversion symmetry which reduces both CPU time and computer memory requirements. In order to accommodate the lattice mismatch between the metal substrate and the *h*-BN monolayer in the *h*-BN/Rh(111) and *h*-BN/Ru(001) interfaces the unit cell contains a 12×12 supercell of the Rh(111) or Ru(001) surface cell and a 13×13 supercell of *h*-BN. For the *h*-BN/Pt(111) system we have used 9×9 Pd and 10×10 *h*-BN supercells.

The atomic structure of the *h*-BN layer in the *h*-BN/TM interfaces is determined by the interaction of the metal substrate with N and B atoms as well as by the interaction between N and B in the overlayer. It has been shown already in the case of the flat *h*-BN deposited on top of a Ni surface that the N atoms are pushed away from the surface whereas the B atoms are attracted to the surface.[23] This explains the observed buckling of about 0.1 Å of the B-N bonds.[3] In cases where the BN and TM lattices do not match, the BN positions vary with respect to the TM atoms. The attractive and repulsive forces depend quite strongly on the actual position of the N or B atoms over the metal surface and result in a large corrugation of the *h*-BN layer. The whole *h*-BN layer is however stabilized by strong sp^2 bonds between B-N atoms which tend to keep *h*-BN as flat as possible. Figure 1 shows the *ab initio* relaxed distance of the N atoms from a flat TM layer in Ru, Rh, and Pt nanomeshes. The B atoms show a very similar pattern but are shifted in some regions by about 0.1 Å toward the metal surface. In all three cases we see two distinct regions where *h*-BN stays close to the metal (light gray) or is far away from it (dark gray). The former region develops around the bonding (B-fcc, N-top) *h*-BN configuration, the latter around nonbonding configurations (B-top, N-hcp and B-hcp, N-fcc).[23] The main differences between these interfaces are related to the size of these bonded and

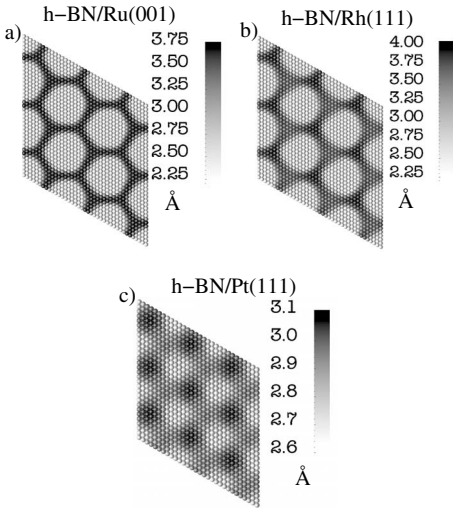

FIG. 1. The distance of the N atoms from the flat metal surface for (a) *h*-BN/Ru(001), (b) *h*-BN/Rh(111), and (c) *h*-BN/Pt(111) interfaces. Note that the plots show 3×3 supercell of the nanomesh unit cells.

nonbonded regions. For the *h*-BN/Ru(001) interface only a relatively small fraction of the *h*-BN layer is pushed away from the surface, about 60% of the N atoms have a z coordinate below the average value. For *h*-BN/Rh(111) this is 54%, whereas for *h*-BN/Pt(111) the fraction drops to 34%. This result agrees perfectly with the conclusions of Preobrajenski *et al.*[26] In the bonding region the average distance of the *h*-BN layer from the metal surface is noticeably smaller for Rh and Ru than for the Pt interface. This reflects the trends in the binding energies of *h*-BN layer to the TM surface calculated in 1×1 commensurate geometries.[32] At the same time the corrugations of the whole *h*-BN layer for the Rh and Ru interfaces are close to 1.9 and 1.6 Å, respectively, and exceed considerably the corrugation of 0.5 Å found for the Pt interface. In the case of *h*-BN/Rh(111) the calculated corrugation is considerably larger than the one reported earlier.[23,24] In Ref. 23 the geometry of the overlayer was calculated using a force field model generated from a set of calculations using commensurate models with 1×1 unit cells, where the *h*-BN bonds have been stretched such that they match with the metal unit-cell size. The stretching of the *h*-BN applied there only slightly affects the electronic structure of the overlayer, but it is enough to change the balance between the attraction of the B atoms and the repulsion of the N atoms and considerably shift the stable equilibrium position of the *h*-BN units in the nonbonding regions. In Ref. 24 the same *ab initio* approach was used as in the present investigation. The geometry optimization was initiated from flat *h*-BN layer and stopped after forces have dropped below 10 mRy/a.u. However the overlayer in the nonbonding regions appears to be extremely soft in the direction perpendicular to the metal surface and the remaining small forces affect considerably the BN-metal distance in those regions. As we already mentioned the atomic structure of the overlayer is a result of the balance between forces acting on N and B atoms that are of opposite sign and the forces acting within *h*-BN plane that tend to keep its planar structure. This

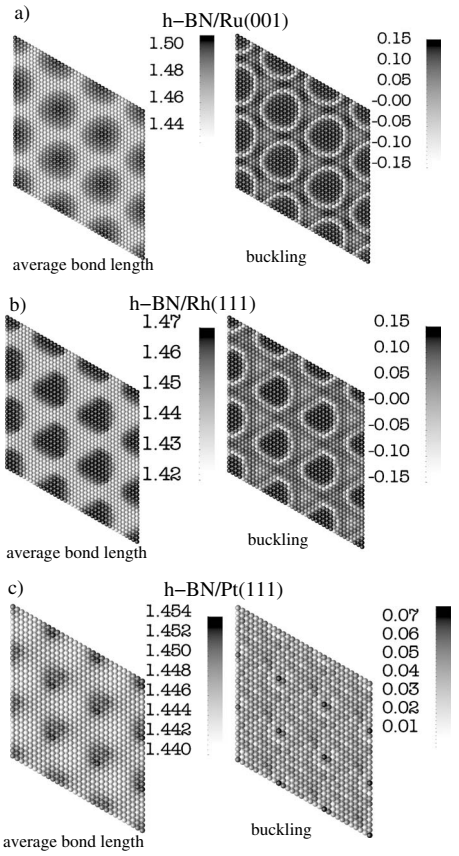

FIG. 2. The average B-N bond length (left column) and the buckling in the N-B_3 unit (right column) for (a) *h*-BN/Ru(001), (b) *h*-BN/Rh(111), and (c) *h*-BN/Pt(111). The buckling is defined as a distance of the N atom to the plane spanned by the three B atoms forming N-B_3 pyramid. Note that the plots show 3×3 supercell of the nanomesh unit cells.

results in a quite long-range effective repulsion of the overlayer in the nonbonded regions. In order to achieve a stable geometry structure and speed up the geometry optimization within the *ab initio* approach, we have initially corrugated the *h*-BN overlayer by about 1.5 Å and monitor its change during the calculation. In order to test the influence of the choice of the DFT on the final geometry we have also calculated the geometry using the LDA.[33] In this case the results are similar to the one computed with the WC-GGA functional.

Although the corrugation is the most spectacular fingerprint of the nanomesh structures, the deformation of the *h*-BN layer can also be visualized by using parameters other than the distance of the N or B atoms to the TM surface. For example, as shown in Fig. 2, the BN bond length and the buckling also follow the nanomesh template. It is rather interesting that for Ru(001) and Rh(111) nanomeshes the average bond length in the NB_3 unit in the bonded region is about 0.05 Å longer than in the nonbonding regions. The differences are much smaller but still visible for *h*-BN/Pt(111). The variation of the bond length across the nanomesh unit cell is a consequence of the fact that the N atoms try to stay as long as possible above the TM atoms. The buckling, defined as the distance between the N atom and the plane

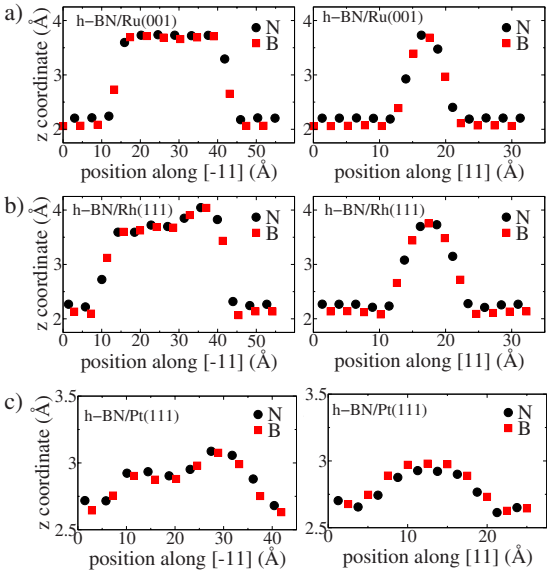

FIG. 3. (Color online) The distance of the N and B atoms from the metal surface for (a) *h*-BN/Ru(001), (b) *h*-BN/Rh(111), and (c) *h*-BN/Pt(111) interfaces plotted for BN units along the $(\bar{1}1)$ direction (long diagonal of the nanomesh unit cell) and the (11) direction (short diagonal).

spanned by the three neighboring B atoms, shows a more complicated pattern. It clearly emphasizes the edge between the relatively flat "low" and "high" regions. As we can see in Fig. 2 the NB_3 units show a negative buckling (in average the N atom is below the plane spanned by the B atoms) at the border between bonding and nonbonding regions, while everywhere else the buckling is positive. In order to visualize the changes of the BN positions between low and high regions more clearly we show the profiles of the BN layer along the longer and shorter diagonals of the nanomesh unit cell in Fig. 3. It can be seen that the BN bonds are very strongly deformed in the rim areas (on the slope). Clearly in the *h*-BN/Rh(111) and *h*-BN/Ru(001) nanomeshes the transition from low to high regions is not a smooth modulation of the flat *h*-BN, but it has a rather steplike character and within one "N-B-N" unit the transition is more or less completed. As can be seen from the right-hand side of Fig. 3 the high regions of the Rh and Ru nanomeshes are very narrow and only three to five atoms wide, while the broad low region is completely flat besides the characteristic BN buckling of about 0.15 Å. On the other hand for the *h*-BN/Pt(111) system the small corrugation is more or less smoothly distributed over the whole unit cell.

The binding energies of the corrugated *h*-BN layer to the metal surface in *h*-BN/Ru(001), *h*-BN/Rh(111), and *h*-BN/Pt(111) nanomeshes are equal to 0.33, 0.25, and 0.070 eV/BN, respectively. These numbers are smaller than the one estimated for commensurate interfaces[32] because a part of the *h*-BN layer is in the nonbonding position over the metal surface, and there is an extra energy cost due to its distortion. The energy losses due to the corrugation of the *h*-BN layer have been estimated by comparing total energies of the isolated flat *h*-BN and the isolated corrugated *h*-BN layer and are equal to 0.124, 0.042, and 0.014 eV for *h*-BN/Ru(001),

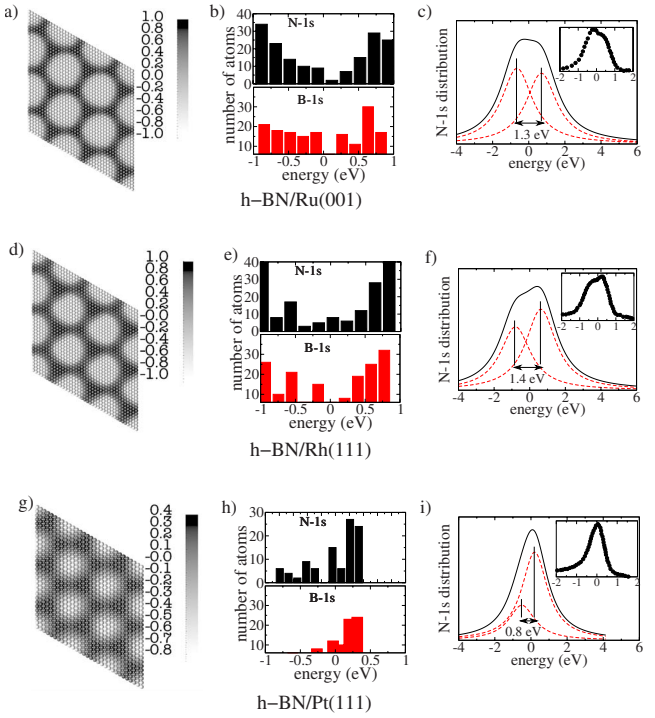

FIG. 4. (Color online) (a) The distribution the N 1*s* core energy levels for *h*-BN/Ru(001) within the nanomesh unit cell, (b) the histogram of the energy distribution of 1*s* core levels for N and B atoms calculated for *h*-BN/Ru(001), and (c) the energy distribution from (b) convoluted with 1-eV-wide Lorentzian peaks (black continuous curve) and its two peak fit (red dashed peaks). (d)–(f) and (g)–(i) like (a)–(c) but for *h*-BN/Rh(111) and *h*-BN/Pt(111), respectively. Insets (a), (f), and (i) show the experimental PES from Ref. 26. Note that the plots in (a), (d), and (g) show 3×3 supercell of the nanomesh unit cells.

h-BN/Rh(111), and *h*-BN/Pt(111) per BN, respectively. Interestingly, a noncommensurate but flat *h*-BN layer does not bind at all to Ru(001) and Rh (111), and in the case of Pt(111) we observe only small binding of approximately 0.015 eV/BN. This clearly shows that the corrugation of the *h*-BN is essential for the stabilization of the interfaces.

B. Electronic structure of the overlayer

The deformation of the *h*-BN overlayer introduces also a variation of the electronic structure in the different regions of the nanomesh unit cell. Such variations affect deep core states as well as the valence bands. In Fig. 4 we show the distribution of the N and B 1*s* core levels in the nanomesh unit cell for all three interfaces. As we can see in Figs. 4(a), 4(d), and 4(g) the distributions follow exactly the nanomesh like pattern displayed in Fig. 1. For all three interfaces the whole *h*-BN overlayer separates into two distinct regions, each one with different but almost rigid shifts of the core levels. The maximal splitting (the difference between the lowest and highest values of the core level) in *h*-BN/Rh(111) and *h*-BN/Ru(001) is about 2 eV, while for the Pt case it is only about 1.2 eV. The main difference between these cases is clearly the shape of the energy distribution of the levels

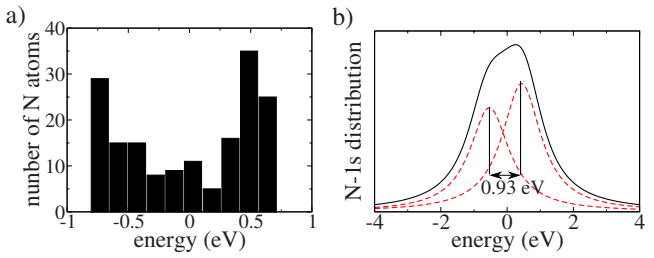

FIG. 5. (Color online) (a) the histogram of the energy distribution of 1*s* core levels for N atoms calculated for *h*-BN/Rh(111) with a BN corrugation of *h*-BN of 0.7 Å; (b) the energy distribution from (a) convoluted with 0.7-eV-wide Lorentzian peaks (black full line) and its two peak fit (red dashed line).

shown in Figs. 4(b), 4(e), and 4(f). For *h*-BN/Rh(111) and *h*-BN/Ru(001) the core levels localize around the high and low ends of the energy distribution. Whereas for *h*-BN/Pt(111) the high energy region dominates. We notice here that the calculated core level splitting seems to be much larger than the one estimated with PES by Preobrajenski *et al.*,[26] which has a similar value of 0.7 eV for all measured substrate. We have checked that this difference is not related to the final state effects. The calculations including core holes resulted in a rigid shift of states in the whole overlayer with unchanged energy distribution of the core levels. However, the apparent disagreement may be partially removed if we convolute our distribution from Figs. 4(b), 4(e), and 4(h) with Lorentzians and then fit the broadened spectrum using only two peaks, as shown in Figs. 4(c), 4(f), and 4(i). This analysis brings our results in much closer agreement with experiment. Our final splittings are about 1.3 eV for *h*-BN/Rh(111) and *h*-BN/Ru(001) and 0.8 eV for *h*-BN/Pt(111). Except for the larger splitting, the shapes of the theoretical convoluted curves resemble the experimental results of Preobrajenski *et al.*[26] pretty well.

The too wide distribution of the 1*s* levels is directly related to the size of the corrugation predicted by the WC-GGA. Figure 5 presents the raw distribution as well as the convoluted distribution generated for *h*-BN/Rh(111) with a corrugation of only 0.7 Å. In this case the distribution is about 50% narrower; the convoluted curve can be fitted with peaks separated by only 0.93 eV, which is fairly close to the 0.7 eV seen in experiments.

The valence states, similarly to the core levels, also follow the nanomesh pattern showing the appropriate splitting of the eigenvalues. We have visualized it by plotting the N $p_{x,y}$ and B $p_{x,y}$ projected density of states (DOS) separately for those N or B atoms that have a z coordinate lower or higher than the average z coordinate of the N or B atoms in the whole *h*-BN overlayer, respectively. The corresponding DOS is shown in Fig. 6. The shape of the DOS for low and high regions is roughly similar. However, they are shifted relative to each other; the DOS in the low region occupies slightly lower energies. The estimated shift between these regions depends on the substrate and varies from approximately 1.0 eV for Rh(111) and Ru(001) to 0.6 eV for Pt(111). The shift for B $p_{x,y}$ seems to be slightly larger than the one for N $p_{x,y}$. Experimentally such a shift has been observed in ultraviolet photoemission spectroscopy (UPS) for the

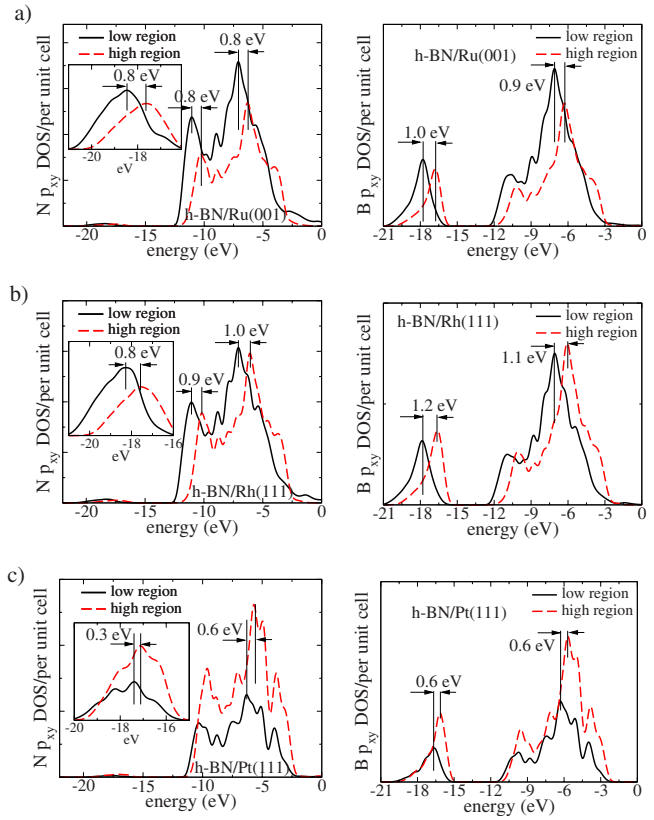

FIG. 6. (Color online) N $p_{x,y}$ (left column) and B $p_{x,y}$ (right column) projected density of states calculated for (a) *h*-BN/Ru(001), (b) *h*-BN/Rh(111), and (c) *h*-BN/Pt(111) interfaces. The contributions from N atoms that are closer to the metal surface than the average (low region) and more distant than the average (high region) are plotted separately. The insets magnify the small peaks in the low energy regions of the N $p_{x,y}$ DOS.

h-BN/Rh(111) interface[12] as an approximately 1 eV splitting of a peak related to the *h*-BN σ band. It was first interpreted as the main evidence for the double layer model of the *h*-BN nanomesh. Note that our theoretical N $p_{x,y}$ and B $p_{x,y}$ DOSs for the whole layer would not show such a clear splitting of the peaks. The UPS experiment probes mainly states around the Γ point in the small *h*-BN unit cell, but in our calculation we are taking into account all backfoldings due to the 13 $\times$ 13 *h*-BN supercell. However, since the σ bands have their minimum or maximum at Γ, we can consider the low energy peaks of our DOS to be representative for the experimental σ band splitting. Interestingly a valence band splitting has not been reported for *h*-BN/Pt(111).[9] The reason for that is probably the relatively small weight related to the elevated region of *h*-BN layer in this interface as seen in Fig. 6(c).

The observed shift of the eigenvalues between low and high regions of the nanomesh is related to the charge transfer between the metal layer and the *h*-BN overlayer. We plot in Fig. 7 the distribution of the total charges inside the atomic spheres for *h*-BN/Rh(111). As we can see, the B and N charges vary by about 0.04*e* and 0.07*e* over the nanomesh unit cell and the B and N have less charge in the regions where the *h*-BN layer is close to the metal surface. The total charge inside the Rh spheres (top layer) shows a larger variation of about 0.12*e*. In addition the Rh atoms that are under the low *h*-BN region have a larger charge than those where *h*-BN is further away. Thus, there is a clear charge transfer from BN toward the Rh atoms. Interestingly, an even larger variation of 0.16*e* appears for the Rh d_{z^2} character, but in the opposite direction, so that it matches the distribution pattern of the N and B charges. Such a behavior can be understood as an effect of hybridization between the Rh *d* and the *h*-BN π orbitals.[32] A direct consequence of this highly nonuniform charge transfer between the metal substrate and the *h*-BN overlayer is a presence of the nonuniform electrostatic field above the interface.[34] As it has already been shown[35] the potential in the hexagonal plane at about 3.8 Å above the *h*-BN layer has a "muffin-tin-like" shape. The difference between the values of the potential above the low and high *h*-BN regions is close to 0.5 eV, which corresponds to observed shifts of the core and valence eigenvalues between those regions. This feature is rather essential for the understanding of the mechanism of trapping of molecules and atoms by the *h*-BN nanomeshes.

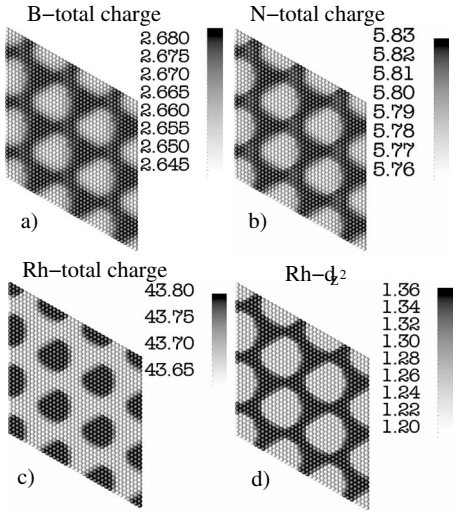

FIG. 7. (a)–(c) The distribution of the total B, N, and Rh charges inside the atomic spheres for *h*-BN/Rh(111). (d) shows the distribution of Rh d_{z^2} electrons only. Note that the plots show 3 $\times$ 3 supercell of the nanomesh unit cells.

III. CONCLUSIONS

To conclude, we have presented results of *ab initio* calculations of the *h*-BN/Ru(001), *h*-BN/Rh(111), and *h*-BN/Pt(111) interfaces. Considering the atomic structure it is clear that in the first two interfaces the *h*-BN layers are rather strongly bound to the TM metal surface, while with Pt(111) the interaction is much weaker. The strength of the interaction manifests itself in both the average distance between the overlayer and the metal surface, as well as in the size and shape of the corrugation of the overlayer. Apparently the calculated corrugation for *h*-BN/Rh(111) is larger than the one in *h*-BN/Ru(001). However in the Ru(001) nanomesh the size of the low (or bonding region) exceeds the one in Rh(111), which may be the reason for the slightly

smaller corrugation in Ru(001), as the strain in the BN bonds is larger in this case. The calculated magnitude of the corrugation reaches almost 2 Å in these two cases, and it is not very reliable because of deficiencies of DFT. All interfaces show a splitting of the core and valence eigenvalues between low and high regions. However, the 1*s* core level splitting is larger for Rh and Ru than for Pt. The valence states localized in the bonding regions [where *h*-BN is close to the metal surface and located around the (B-fcc, N-top) configuration] are shifted by about 0.8 eV relatively to the nonbonding (high) regions. As we have shown such a shift of eigenvalues is related to the nonuniform charge transferred to the *h*-BN layer and consequently the presence of nonuniform electrostatic field above the layer.

ACKNOWLEDGMENTS

We acknowledge support from Austrian Science Foundation (FWF), Grant No. I319-N20. The calculations were carried out at the Vienna Scientific Cluster.

[1] A. Nagashima, N. Tejima, Y. Gamou, T. Kawai, and C. Oshima, Phys. Rev. B **51**, 4606 (1995).
[2] A. B. Preobrajenski, A. S. Vinogradov, and N. Mårtensson, Surf. Sci. **582**, 21 (2005).
[3] G. B. Grad, P. Blaha, K. Schwarz, W. Auwärter, and T. Greber, Phys. Rev. B **68**, 085404 (2003).
[4] A. B. Preobrajenski, A. S. Vinogradov, and N. Mårtensson, Phys. Rev. B **70**, 165404 (2004).
[5] A. Nagashima, N. Tejima, Y. Gamou, T. Kawai, and C. Oshima, Phys. Rev. Lett. **75**, 3918 (1995).
[6] S. Berner *et al.*, Angew. Chem., Int. Ed. Engl. **46**, 5115 (2007).
[7] A. Goriachko, Y. He, M. Knapp, and H. Over, Langmuir **23**, 2928 (2007).
[8] M. T. Paffett, R. J. Simonson, P. Papin, and R. T. Paine, Surf. Sci. **232**, 286 (1990).
[9] A. B. Preobrajenski, A. S. Vinogradov, M. L. Ng, E. E. Ćavar, R. Westerström, A. Mikkelsen, E. Lundgren, and N. Mårtensson, Phys. Rev. B **75**, 245412 (2007).
[10] F. Müller, K. Stöwe, and H. Sachdev, Chem. Mater. **17**, 3464 (2005).
[11] M. Morscher, M. Corso, T. Greber, and J. Osterwalder, Surf. Sci. **600**, 3280 (2006).
[12] M. Corso, W. Auwärter, M. Muntwiler, A. Tamai, T. Greber, and J. Osterwalder, Science **303**, 217 (2004).
[13] A. Goriachko, Y. He, and H. Over, J. Phys. Chem. C **112**, 8147 (2008).
[14] M. L. Ng, A. B. Preobrajenski, A. Vinogradov, and N. Mårtensson, Surf. Sci. **602**, 1250 (2008).
[15] I. Brihuega, C. Michaelis, J. Zhang, S. Bose, V. Sessi, J. Honolka, M. Schneider, A. Enders, and K. Kern, Surf. Sci. **602**, L95 (2008).
[16] A. T. N'Diaye, S. Bleikamp, P. J. Feibelman, and T. Michely, Phys. Rev. Lett. **97**, 215501 (2006).
[17] S. Marchini, S. Günther, and J. Wintterlin, Phys. Rev. B **76**, 075429 (2007).
[18] A. B. Preobrajenski, M. L. Ng, A. S. Vinogradov, and N. Mårtensson, Phys. Rev. B **78**, 073401 (2008).
[19] T. Brugger, S. Günther, B. Wang, H. Dil, M.-L. Bocquet, J. Osterwalder, J. Wintterlin, and T. Greber, Phys. Rev. B **79**, 045407 (2009).
[20] E. D. L. Rienks, N. Nilius, H. P. Rust, and H. J. Freund, Phys. Rev. B **71**, 241404(R) (2005).
[21] F. Müller, S. Hüfner, and H. Sachdev, Surf. Sci. **602**, 3467 (2008).
[22] M. P. Allan, S. Berner, M. Corso, T. Greber, and J. Osterwalder, Nanoscale Res. Lett. **2**, 94 (2007).
[23] R. Laskowski, P. Blaha, T. Gallauner, and K. Schwarz, Phys. Rev. Lett. **98**, 106802 (2007).
[24] R. Laskowski and P. Blaha, J. Phys.: Condens. Matter **20**, 064207 (2008).
[25] F. Müller, S. Hüfner, and H. Sachdev, Surf. Sci. **603**, 425 (2009).
[26] A. B. Preobrajenski, M. A. Nestrov, M. L. Ng, A. S. Vinogradov, and N. Mårtensson, Chem. Phys. Lett. **446**, 119 (2007).
[27] P. Blaha, K. Schwarz, G. K. H. Madsen, D. Kvasnicka, and J. Luitz, *WIEN2K, An Augmented Plane Wave Plus Local Orbitals Program for Calculating Crystal Properties* (Vienna University of Technology, Vienna, 2001).
[28] G. K. H. Madsen, P. Blaha, K. Schwarz, E. Sjöstedt, and L. Nordström, Phys. Rev. B **64**, 195134 (2001).
[29] Z. Wu and R. E. Cohen, Phys. Rev. B **73**, 235116 (2006).
[30] F. Tran, R. Laskowski, P. Blaha, and K. Schwarz, Phys. Rev. B **75**, 115131 (2007).
[31] P. Haas, F. Tran, and P. Blaha, Phys. Rev. B **79**, 085104 (2009); **79**, 209902(E) (2009).
[32] R. Laskowski, P. Blaha, and K. Schwarz, Phys. Rev. B **78**, 045409 (2008).
[33] J. P. Perdew and Y. Wang, Phys. Rev. B **45**, 13244 (1992).
[34] T. Greber, M. Corso, and T. Osterwalder, Surf. Sci. **603**, 1373 (2009).
[35] H. Dil, J. Lobo-Checa, R. Laskowski, P. Blaha, S. Berner, J. Osterwalder, and T. Greber, Science **319**, 1824 (2008).